Bridge-Mediated Metal-to-Metal Electron and Hole Transfer in Supermolecular Dinuclear Complex: A Computational Study using Quantum Electron-Nuclear Dynamics

Xiaolin Liu,[†] Dugan Hayes,[‡] Lin X. Chen,[¶] and Xiaosong Li[*,†]

[†]*Department of Chemistry, University of Washington, Seattle, WA 98195, USA*

[‡]*Department of Chemistry, University of Rhode Island, Kingston, RI 02881, USA*

[¶]*Chemical Sciences and Engineering Division, Argonne National Laboratory, Lemont, IL 60439, USA; Department of Chemistry, Northwestern University, Evanston, IL 60208, USA*

E-mail: xsli@uw.edu

Abstract

Bimetallic electron donor-acceptor complexes can facilitate electron and energy transfer with excellent structural control through synthetic design. In this work, we investigate the photochemical dynamics in a Ru-Cu bimetallic complex after photoexcitation of the Ru-centered charge transfer state. The physical underpinnings of the metal-to-metal directional charge transfer process are unraveled via analyses of the quantum electronic dynamics and electron-nuclear trajectories. The effects of molecular vibrations in the photoexcited state on the charge transfer processes are also analyzed.

1 Introduction

Inspired by molecules in natural photosynthesis, much attention has focused on the rational design of molecular complexes with multiple transition metal centers. Bimetallic electron donor-acceptor complexes are the simplest among them and are ideal molecular architectures for incorporating building blocks of transition metal chromophores. Tetrapyrido[3,2-a:2′,3′-c:3″,2′-h:2‴,3‴-j]phenazine (tpphz, Figure 1) has been used as the bridging ligand in the design and synthesis of bimetallic complexes, since the extended π system can potentially facilitate electron and energy transfer between metal centers.[1,2] The excited state dynamics of polypyridyl dinuclear complexes with a tpphz bridging ligand have been extensively studied. Flamigni *et al.* studied a Ru(II)-Ru(II) dinuclear complex bridged by tpphz and revealed that there is an excited state interconversion between two metal-to-ligand charge transfer (MLCT) states.[3] Chiorboli and coworkers investigated the photophysical properties and solvent-dependent excited state decay dynamics of homo- and heterodinuclear complexes with Ru and Os centers.[4,5] The ultrafast intramolecular electron transfer in a Ru(II)-Co(III) complex has been studied using transient optical and X-ray spectroscopies.[6–8]

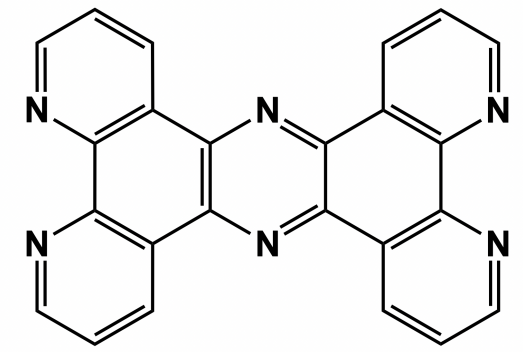

Figure 1. Structure of the tetrapyrido[3,2-a:2′,3′-c:3″,2′-h:2‴,3‴-j]phenazine (tpphz) ligand.

The synthetic strategy of CuHETPHEN (Cu(I) heteroleptic bis(1,10-phenanthroline)) has been used extensively in recent years because it provides exquisite structural control in the assembly of heteroleptic (and thus multi-functional) complexes with earth-abundant

copper.[9–14] Combining the idea of using tpphz as a bridging ligand and the CuHETPHEN strategy, Hayes *et al.* synthesized a group of mononuclear and homo- and heterodinuclear complexes with Cu and/or Ru centers. Experimental studies using optical and X-ray transient absorption spectroscopy suggest that the bridging ligand in such bimetallic complexes plays an important role in the directional photoexcited charge transfer in addition to the redox properties of the metal centers.[13,15] This observation provides an important rational design principle for steering photochemical processes in bimetallic electron donor-acceptor complexes. Understanding the dynamics of photochemical processes and the interplay between ligands and metal centers is key to engineering high-efficiency solar cells and photocatalysts.[15–18] Theory and computation, especially modern time-dependent quantum electronic dynamics, as complementary tools to spectroscopic probes, can provide atto- to femtosecond-resolved physical insights into the electronic and structural characteristics underlying experimental observations.[19,20]

In this work, we provide quantum mechanical insights into the ultrafast electronic and vibrational dynamics that underpin the directional photoexcited charge transfer in a bimetallic electron donor–bridge-acceptor complex. We seek to understand how the bridge and other metal-bound ligands modulate the excited state dynamics that results in the highly efficient directional charge transfer event.

2 Methodology

2.1 Real-Time Time-dependent Density Functional Theory and Ehrenfest Dynamics

In ultrafast photochemical dynamics, electronic degrees of freedom are in the non-equilibrium condition. Simulating such photochemical processes requires treatments of electronic coherence as well as non-equilibrium non-adiabatic energy transfer pathways.[19,20] The high density-of-excited-states nature of the molecular systems of interest makes Ehrenfest dynam-

ics an ideal approach to simulate quantum dynamics within the time-dependent Schrödinger equation framework. In this work, we carried out *ab initio* on-the-fly Ehrenfest dynamics in the atomic orbital basis[21–26] to simulate the ultrafast electron-hole dynamics and their interplay with molecular vibrations.

As the *ab initio* Ehrenfest dynamics method has been previously developed and applied to modeling various ultrafast excited state electron-nuclear dynamics, we provide only a brief review of it here. We refer readers to recent reviews[19,20] for theoretical details. In *ab initio* Ehrenfest dynamics, the electronic degrees of freedom are explicitly propagated with real-time time-dependent density functional theory (RT-TDDFT). The electron-nuclear interactions responsible for the electronically non-adiabatic time evolution are modeled with the Ehrenfest technique, which propagates the nuclei on the time-evolving electronic potential.

The Ehrenfest dynamics scheme employed in this work takes advantage of an efficient triple-split operator integrator.[21] These different time steps reflect the characteristic timescales of the three different molecular equations-of-motion: nuclear motion driven by the velocity-Verlet algorithm with a time-step of Δt_N, the evolving time-dependent Kohn-Sham Hamiltonian with a time-step of Δt_{Ne}, and a unitary transformation RT-TDDFT used to propagate the electronic degrees of freedom with a time-step of Δt_e.

2.2 Initial Condition and Population Analysis

The photochemical dynamics start from the photoexcited MLCT state. A linear response TDDFT calculation suggests that the metal-to-ligand charge transfer transition involves several ligand orbitals. To facilitate the population analysis and prepare the initially photoexcited MLCT state, canonical orbitals are transformed to the natural transition orbitals (NTOs).[27,28] The total number of electrons is conserved in the process because the NTO transformation is unitary. In the NTO description, the MLCT excitation becomes a one-electron transition between orbitals. Therefore, the initial density at $t = 0$ fs is prepared by

promoting one electron from the highest occupied to the lowest unoccupied NTO, resulting a density matrix in the NTO basis. All occupied NTOs are used in constructing the one-electron density matrix and all NTOs are used in the population projection analysis. The NTO density matrix is transformed into the atomic orbital basis to initialize the quantum electron and electron-nuclear dynamics.

The on-the-fly population analysis is also carried out in the NTO basis. The time-dependent electron density matrix $\mathbf{P}(t)$ is projected to the ground state NTOs $\mathbf{C}_i$ computed at $t = 0$ and the occupation number of the i-th NTO is calculated as:

$$n_i(t) = \mathbf{C}_i(0)^\dagger \mathbf{P}(t) \mathbf{C}_i(0). \tag{1}$$

Note that population projection to the $t = 0$ ground state NTO space is valid only when the molecular geometry does not change in time.

3 Results and Discussion

All calculations were performed using a developmental version of the Gaussian software package.[29] The geometry of the bpy-Ru-tpphz-Cu-dmesp molecule (CuH_2-RuH_2 for short, Figure 2) molecule was optimized using the M06 functional[30] including Grimme's D3 dispersion.[31] The ultrafine grid option is used for the DFT numerical integration in the linear response TDDFT calculations. For quantum dynamics simulations, the fine grid option is employed. The LANL2DZ ECP basis[32] for Cu and Ru and SBJKC-VDZ basis[33,34] for light atoms were used in the geometry optimization. The Ehrenfest quantum dynamics calculations were performed using the same functional and basis sets. These basis sets were chosen because they reproduce important characteristics of the molecular geometry and UV-Vis spectrum calculated using a larger basis set but with a much lower computational cost for quantum dynamics (see Figure S1 and S2 in the SI). The step size of electronic dynamics is set to 0.0012 fs. The time steps in Ehrenfest dynamics are: $\Delta t_N = 0.15$ fs, $\Delta t_{Ne} = 0.015$ fs,

and $\Delta t_e = 0.0015$ fs, according to the triple-split operator scheme.[21] Both dynamics were simulated for ∼200 fs.

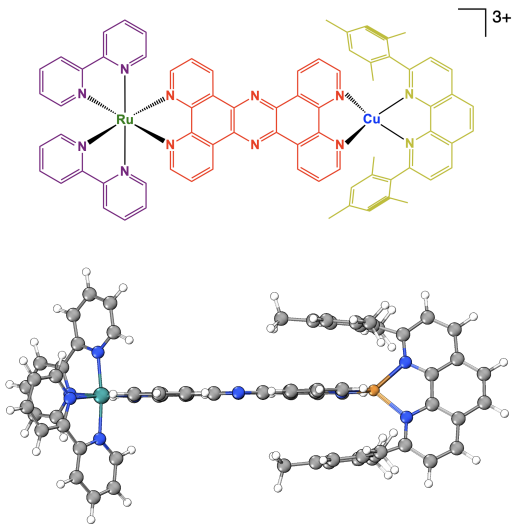

Figure 2. Structure of the bpy-Ru-tpphz-Cu-dmesp (CuH_2-RuH_2 for short) molecule. The 2,2′-bipyridine (bpy) ligands are shown in purple; the tetrapyrido[3,2-a:2′,3′-c:3″,2′-h:2‴,3‴-j]phenazine (tpphz) bridge is shown in red; and the 2,9-dimesityl-1,10-phenanthroline (dmesp) ligand is shown in yellow.

3.1 Ground State Geometry and UV-Vis Spectrum

The optimized geometry of the CuH_2-RuH_2 bimetallic molecule is shown in Figure 2. The Ru atom bonds to two 2,2′-bipyridine (bpy) ligands and one side of the tpphz ligand. The Cu atom bonds to the 2,9-dimesityl-1,10-phenanthroline (dmesp) ligand and the other side of the tpphz ligand. To simplify notations, the molecule can be grouped into five parts: bpy-Ru-tpphz-Cu-dmesp. On the Cu-side of the structure, the two mesityl groups of the dmesp ligand are almost parallel to the tpphz ligand, suggesting strong $\pi-\pi$ interaction between ligand and bridge, similar to the "pac-man" motif in other Cu(I)-centered HETPHEN complexes.[15,35,36] The methyl substituents at 2,6-positions of the aryl groups prevent the dmesp ligand from rotating, resulting in a stable $\pi - \pi$ interaction. The bridging ligand remains in a flat configuration that provides an ideal pathway for electron transfer.

The UV-Vis spectrum of CuH_2-RuH_2 computed using linear response TDDFT is shown

in Figure 3. The overall spectrum agrees with the experimental measurement,[15] where there is a broad feature in the 600-400 nm range (1.9∼3.1 eV). This low-energy band consists of MLCT transitions centered around the two metal sites. The lowest energy transitions all originate from the Cu center (see inset for a representative NTO transition pair for a selected Cu-centered MLCT excitation). While the excitations come from Cu 3*d* electrons, there is a dense manifold of accepting ligand orbitals delocalized throughout nearby ligands that give rise to the broad MLCT feature in the experimental spectrum. The Cu-center MLCT band continues to ∼480 nm (∼2.6 eV), where we start to see overlapping contributions from the Ru-centered MLCT excitations. The inset of Figure 3 shows the characteristics of a selected Ru-centered MLCT excitation which has similar characteristics to the Cu-centered band except with the electron excited from the Ru 4*d* orbitals.

In order to quantify the charge transfer characteristics, the molecular system is again divided into five distinct groups as color-coded in Figure 2. Charge transfer matrix analysis[37,38] was carried out to quantify the amount of charge transfer between different molecular motifs. Particularly, this approach allows us to characterize the roles of different ligands (*e.g.*, tpphz, bpy, or dmesp) in the MLCT excitation. Charge transfer strengths are shown in Figure 3 for the selected MLCT transitions. In the Cu MLCT states, the charge moves mostly from Cu and nearby dmesp to the tpphz bridge ligand. For Ru-centered MLCT states, the charge transfer event occurs from Ru-*d* orbital to both the tpphz bridge and nearby bpy ligands. There is also significant inter-ligand charge transfer from the dmesp at the Cu site to the tpphz bridge ligand, similar to that observed for the Cu MLCT states. This observation highlights the long-range electronic coupling present in this system.

3.2 Quantum Electronic Dynamics

The spectral analysis above suggests that the tpphz bridging ligand plays an important role in the charge transfer events at the two metal centers. Cu- and Ru-centered MLCT states are coupled through the tpphz bridging ligand, which may provide an electron transfer

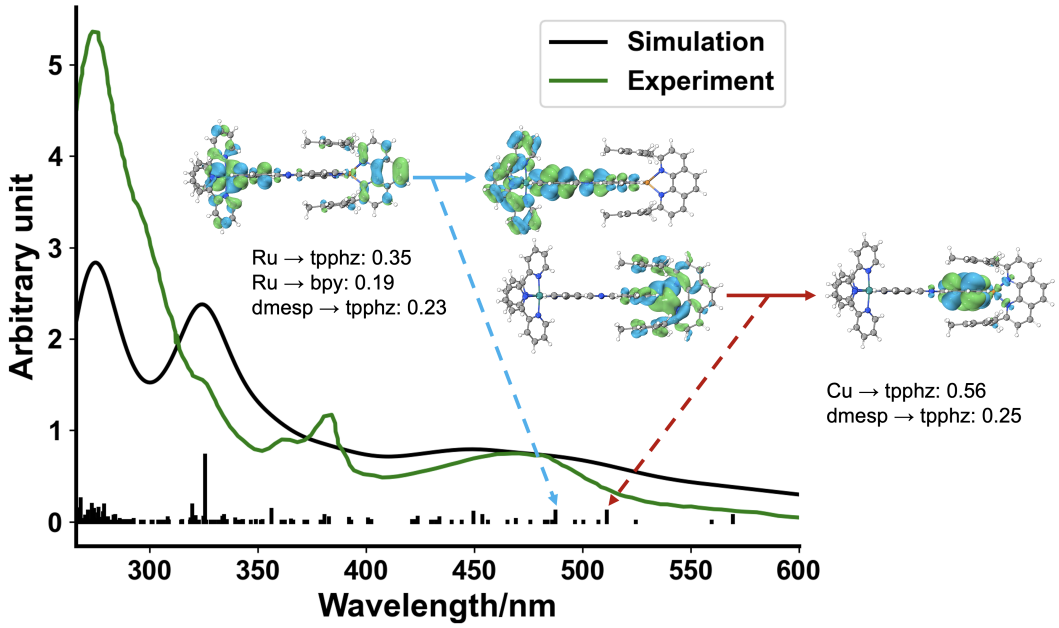

Figure 3. Absorption spectrum of CuH_2-RuH_2 computed using linear response TDDFT. A Lorentzian broadening factor of 0.2 eV is used to plot the simulated spectrum. The experimental spectrum is digitized from Ref. 15. Natural transition orbitals of selected MLCT excitations are displayed with charge transfer matrix elements.

pathway between the two metal centers. In this section, we carry out quantum electronic dynamics simulations to investigate the electron transfer pathways in the bpy-Ru-tpphz-Cu-dmesp bimetallic complex. With the electron-nuclear Ehrenfest dynamics, we also study the molecular structure change in the metal-to-metal charge transfer event.

The photochemical dynamics start from the Ru-center MLCT state prepared according the procedure illustrated in the Methodology section. The Ru-center MLCT state is higher in energy than the Cu-center MLCT level, giving rise to an energetically feasible metal-to-metal charge transfer pathway. The photoexcited state arises from electronic transitions from Ru-d orbitals to the bpy ligands accompanied by charge transfer from dmesp ligand at the Cu site to the tpphz bridge (Figure 4A). After photoexcitation at $t = 0$ fs, the coherent electron-hole recombination takes place within 50 fs, shown in Figure 4A. While the photoexcited hole orbital repopulates to unity, the photoexcited electron does not deplete completely and still has a significant population at $t = 200$ fs. Detailed analysis suggests that the photoexcited

hole receives additional electron populations from other occupied Ru-d orbitals, one of which is shown in Figure 4B. These selected orbital population evolutions shown in Figure 4 carry the important photophysics of interest. While there are some populations in other orbitals, they are considered as electronic structure reorganization in response to the photochemical processes.

The observation illustrated above from electronic dynamic simulations suggests that the photoexcited electron at the tpphz bridge can be persistent. This is because the photoexcited hole is filled quickly by electron transfer from other Ru-d electrons. These faster dynamics prevent a complete electron-hole recombination and therefore lead to a long-lived electron population at the tpphz bridge site and a significant population in the Ru-centered MLCT state. Figure 5 plots the electron density difference snapshots as a function of time (t = 0, 50, and 200 fs) following excitation. It is clear to see there is a significant electron density residing at the tpphz bridge site even at 200 fs.

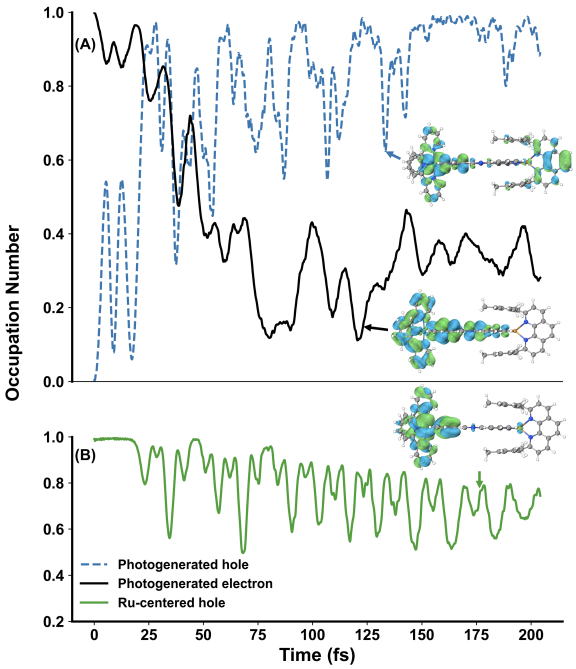

Figure 4. Time evolution of selected orbital populations after photoexcitation at t = 0 fs. Natural transition orbital (NTO) population analysis is carried out according to the procedure described in the Methodology section. NTOs are shown as insets. (**A**) Populations of the photoexcited electron (solid line) and hole (dashed line). (**B**) Population of a Ru-d orbital that transfers electron population to the photoexcited hole.

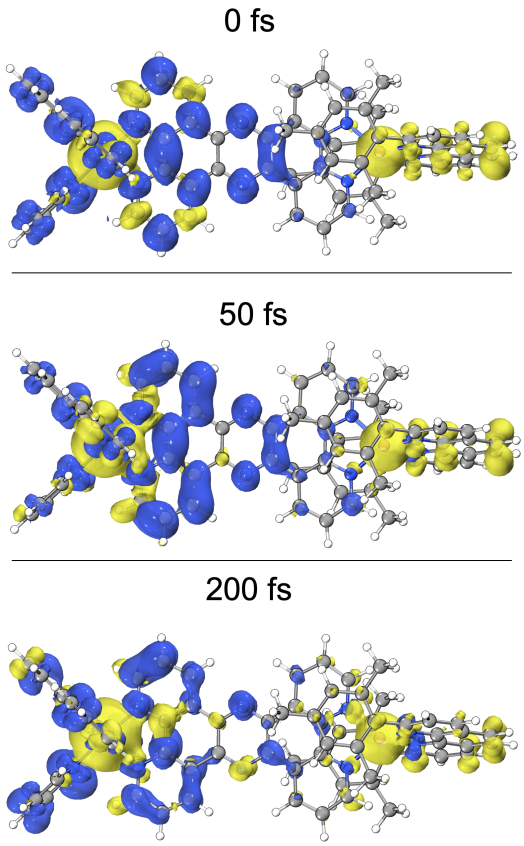

Figure 5. Electron density difference plots at $t = 0$, 50, and 200 fs. Electron density difference is computed as $\Delta\mathbf{P}(t) = \mathbf{P}(t) - \mathbf{P}_0(0)$ where $\mathbf{P}(t)$ is the time-dependent density matrix and $\mathbf{P}_0(0)$ is the ground state densitry matrix at $t = 0$ fs. An isovalue of 0.0004 is used. The blue/yellow color indicates an increased/decreased electron density compared to the ground state at $t = 0$ fs.

3.3 Electron-Nuclear Ehrenfest Dynamics

The dynamics discussed above describe the main electronic characteristics underlying the photoinduced charge transfer event in the bimetallic molecular complex. However, in the absence of nuclear dynamics, photochemical processes are reversible – a scenario that does not sustain directional metal-to-metal charge transfer. In order to understand the interplay between electronic and vibrational degrees of freedom during the charge transfer event and identify key molecular vibrations underlying the directional metal-to-metal charge transfer, we carried out electron-nuclear Ehrenfest dynamics starting from the the same Ru-centered MLCT state. The initial molecular structure is taken as the ground state minimum and

will evolve according to the classical equation of motion on the RT-TDDFT potential energy surface.

Figure 6 shows the geometric changes compared to the initial ground state minimum. Noticeable changes are observed at 30 fs following the photoexcitation. For example, a small opening-closing motion of the mesityl ligands at the Cu site starts to occur. This vibrational motion changes the distance between the mesityl groups and the bridge by $\pm$0.003-0.005Å. In addition, a small out-of-plane vibration of the tpphz bridge ligand is observed with a $\sim$3.5° bending. At around 120 fs, which is the onset of the metal-to-metal electron transfer (MMET, see below) from Cu to Ru, a small rotation of the tpphz ligand along the Cu-Ru axis occurs, indicating a change of dominant vibrational mode. This mode is persistent until the end of our simulation. The rotation of the tpphz ligand can lead to a change of the dihedral angle between the tpphz and the backbone of the dmesp ligand, which is a key geometric feature of Cu(I) excitation. These small geometric changes identified in Figure 6 are possible vibrational driving forces underlying the direction metal-to-metal charge transfer event.

Figure 7 shows the time evolution of charge differences at the Ru, Cu, and tpphz bridge sites computed using the time-dependent densities from the electron-nuclear Ehrenfest dynamics. The charge difference is computed using time-dependent Mulliken population analysis with respect to the ground state at $t < 0$ fs. To better understand the charge transfer pathway, the charge evolutions of the Cu and Ru sides of the tpphz ligand are separately plotted.

Upon photoexcitation at $t = 0$ fs, both sides of the tpphz bridging ligand gain electron population from Ru-centered MLCT excitation. This analysis agrees with the charge transfer matrix elements shown in Figure 3. In the first $\sim$150 fs, two distinct oscillatory charge transfer events are observed, identified by their relative time-evolution phases: fast transfer between the Ru-sided tpphz and Cu-sided tpphz ligand, and slow transfer between Ru-d and Cu-d manifolds. The former is a clear signature of bridge-mediated electron transfer

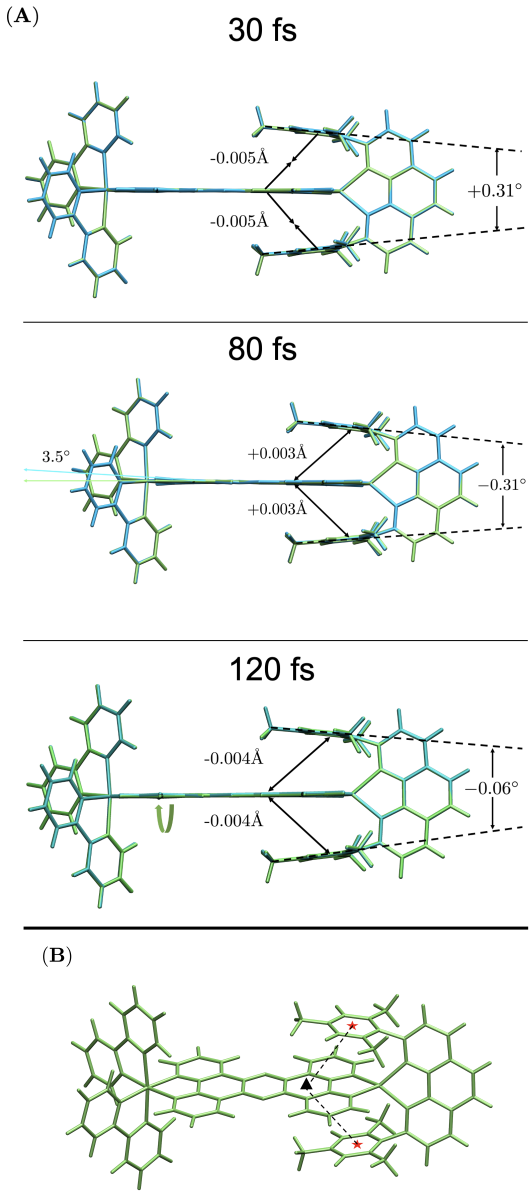

Figure 6. Geometric changes compared to the initial ground state structure. (**A**) Geometries at 30 fs, 80 fs, and 120 fs. The lime-colored molecule is the initial geometry and the cyan-colored are the geometry snapshots from the Ehrenfest dynamics. (**B**) The distance between the mesityl groups and the bridge is measured as the center of the benzene units of the mesityl group (red star) and the tpphz bridge (black triangle).

and the latter can be viewed as direct hole transfer between the metal centers. These two ultrafast charge transfer events are mostly correlated with the closing motion of the mesityl ligands at the Cu site and the rotational motion of the tpphz bridge (see Figure 6). Figure 8 shows the proposed mechanism underlying the observed photochemical process.

After the photoexcitation to the Ru-centered MLCT state, there are concerted electron and hole transfer events taking place between the Ru-centered and Cu-centered MLCT states, giving rise to the characteristic metal-to-metal charge transfer process.

To confirm that these small geometric changes identified in Figure 6 are correlated with direction metal-to-metal charge transfer event, the Mulliken charge differences are Fourier transformed into the frequency domain and the possible vibrational modes that modulate the charge evolutions are shown in Figure 9. Fourier transform of the charge evolution shows that the dominant low frequencies are in the 600 to 900 cm^{-1} range. Analysis of the ground state vibrations identifies several modes that may be responsible for the charge evolution modulation. The 748 cm^{-1} and 796 cm^{-1} vibrational modes correspond to Ru-centered bpy twisting motion which gives rise to the out-of-plane rotation of the Ru-sided tpphz ligand. The 703 cm^{-1} vibrational mode corresponds to Cu-centered dmesp ligand motion (see Figure 6). The 846 cm^{-1} mode is especially interesting because it correlates the motion of Cu and Ru sites with the bridging tpphz ligand. The analysis presented here suggests that the electron and hole transfers can be modulated by ligand motions.

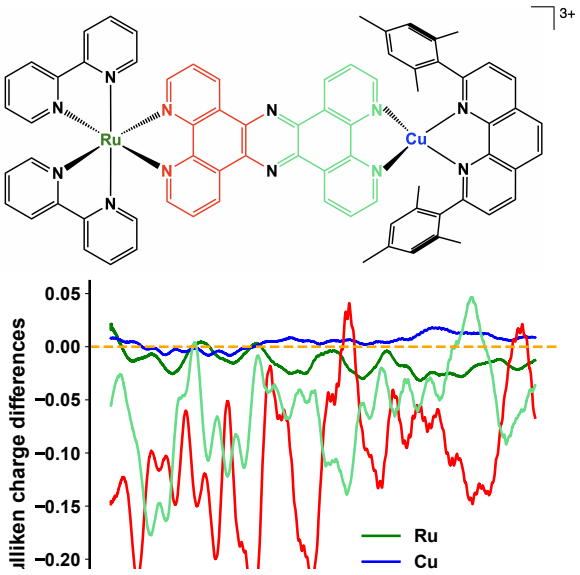

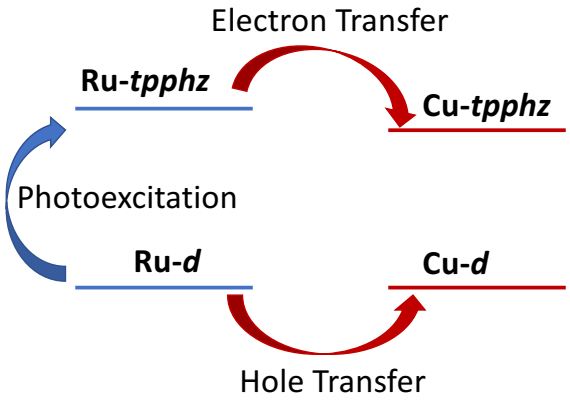

Figure 8. Proposed excited state metal-to-metal charge transfer mechanism.

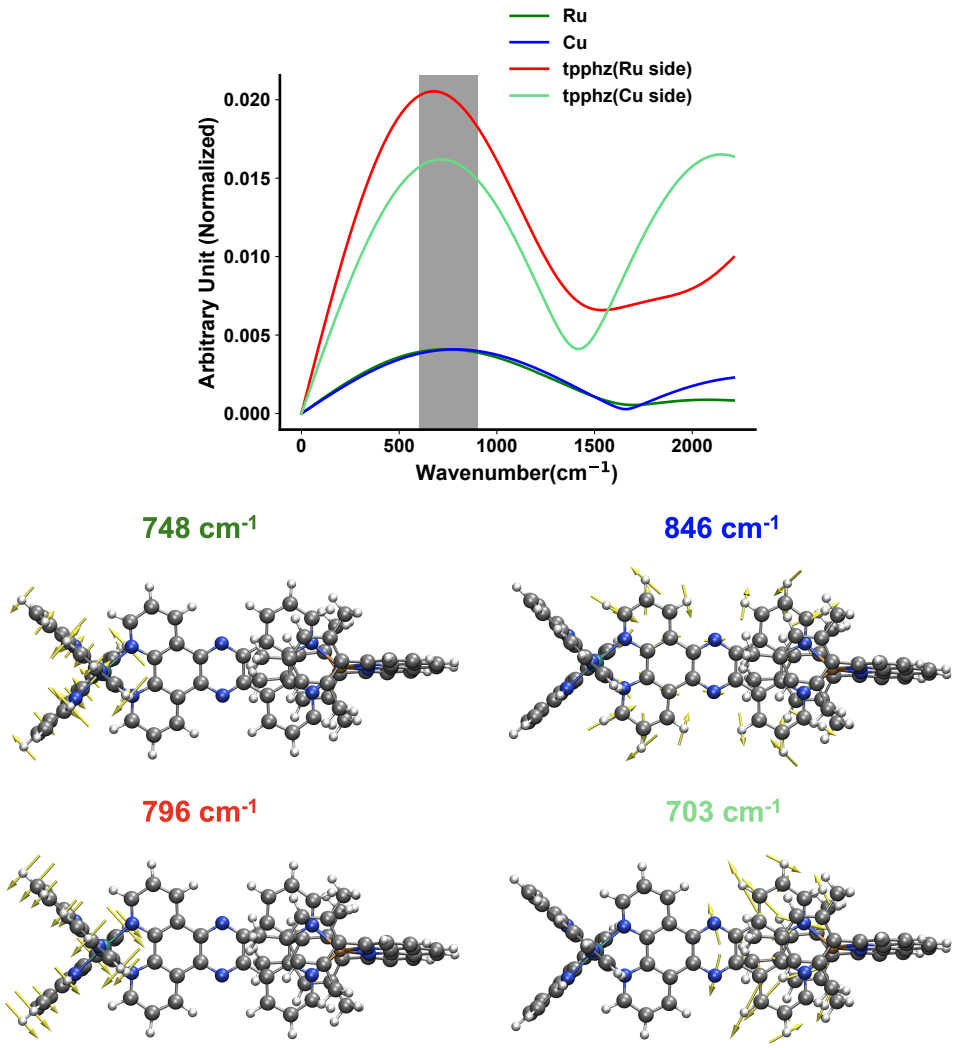

Figure 9. (**Top Panel**): Fourier transform (FT) of the time-evolution of Mulliken change difference. Areas between 600 and 900 cm^{-1} are shaded in grey. (**Bottom Panel**): Ground state vibrational modes in the range of 600-900 cm^{-1} with displacement vectors.

4 Conclusion

In this work, we have applied *ab initio* electron-nuclear dynamics to study the dynamical interplay between two metal-centered charge transfer states in a bimetallic complex. The photochemical dynamics were initiated by photoexcitation of the Ru-centered MLCT state. Electronic dynamics show that although there is a fast partial electron-hole recombination, the Ru-centered MLCT largely remains in its photoexcited state because the Ru-*d* reorga-

nization prevents it from a complete coherent decay to the ground state. Electron-nuclear Ehrenfest dynamics show that the molecular vibrations on the excited state lead to a small rotational motion of the tpphz bridge and closing motion of the mesityl ligands. These vibrational modes are seen to drive the metal-to-metal charge transfer event with both electron and hole populations being transferred in a concerted dynamics.

Acknowledgement

This work was supported by the Ultrafast Initiative of the U. S. Department of Energy, Office of Science, Office of Basic Energy Sciences, through Argonne National Laboratory under Contract No. DE-AC02-06CH11357. The development of time-dependent electronic structure methods is supported by the National Science Foundation (CHE-2154346 to X.L.). Computations were facilitated through the use of advanced computational, storage, and networking infrastructure provided by the Hyak supercomputer system at the University of Washington, funded by the Student Technology Fee.

Supporting Information Available

The supporting information includes: molecular structure; comparison of UV-Vis spectra and molecular structures computed with different basis sets.

References

(1) Knapp, R.; Schott, A.; Rehahn, M. A Novel Synthetic Strategy toward Soluble, Well-defined Ruthenium (II) Coordination Polymers. *Macromolecules* **1996**, *29*, 478–480.

(2) Bolger, J.; Gourdon, A.; Ishow, E.; Launay, J.-P. Mononuclear and Binuclear Tetrapyrido [3,2-a:2′,3′-c:3″,2′-h:2‴,3‴-j] phenazine (tpphz) Ruthenium and Osmium Complexes. *Inorg. Chem.* **1996**, *35*, 2937–2944.

(3) Flamigni, L.; Encinas, S.; Barigelletti, F.; MacDonnell, F. M.; Kim, K.-J.; Puntoriero, F.; Campagna, S. Excited-state Interconversion between Emissive MLCT Levels in a Dinuclear Ru (II) Complex Containing a Bridging Ligand with an Extended π System. *Chem. Commun.* **2000**, *13*, 1185–1186.

(4) Chiorboli, C.; Bignozzi, C. A.; Scandola, F.; Ishow, E.; Gourdon, A.; Launay, J. P. Photophysics of Dinuclear Ru(II) and Os(II) Complexes Based on the Tetrapyrido[3,2-a:2′,3′-c:3″,2′-h:2‴,3‴-j] phenazine (tpphz) Bridging Ligand. *Inorg. Chem.* **1999**, *38*, 2402–2410.

(5) Chiorboli, C.; Rodgers, M. A.; Scandola, F. Ultrafast Processes in Bimetallic Dyads with Extended Aromatic Bridges. Energy and Electron Transfer Pathways in Tetrapyridophenazine-bridged Complexes. *J. Am. Chem. Soc.* **2003**, *125*, 483–491.

(6) Torieda, H.; Nozaki, K.; Yoshimura, A.; Ohno, T. Low Quantum Yields of Relaxed Electron Transfer Products of Moderately Coupled Ruthenium(II)-cobalt(III) Compounds on the Subpicosecond Laser Excitation. *J. Phys. Chem. A* **2004**, *108*, 4819–4829.

(7) Canton, S. E.; Zhang, X.; Zhang, J.; van Driel, T. B.; Kjaer, K. S.; Haldrup, K.; Chabera, P.; Harlang, T.; Suarez-Alcantara, K.; Liu, Y. et al. Toward Highlighting the Ultrafast Electron Transfer Dynamics at the Optically Dark Sites of Photocatalysts. *J. Phys. Chem. Lett.* **2013**, *4*, 1972–1976.

(8) Canton, S. E.; Kjær, K. S.; Vankó, G.; Van Driel, T. B.; Adachi, S.-i.; Bordage, A.; Bressler, C.; Chabera, P.; Christensen, M.; Dohn, A. O. et al. Visualizing the Non-equilibrium Dynamics of Photoinduced Intramolecular Electron Transfer with Femtosecond X-ray Pulses. *Nat. Chem.* **2015**, *6*, 1–10.

(9) Schmittel, M.; Ganz, A. Stable Mixed Phenanthroline Copper (i) Complexes. Key Building Blocks for Supramolecular Coordination Chemistry. *Chem. Commun.* **1997**, 999–1000.

(10) Schmittel, M.; Lüning, U.; Meder, M.; Ganz, A.; Michel, C.; Herderich, M. Synthesis of Sterically Encumbered 2, 9-diaryl Substituted Phenanthrolines. Key Building Blocks for the Preparation of Mixed (bis-heteroleptic) Phenanthroline Copper (I) Complexes. *Heterocycl. Commun.* **1997**, *3*, 493–498.

(11) Sandroni, M.; Kayanuma, M.; Planchat, A.; Szuwarski, N.; Blart, E.; Pellegrin, Y.; Daniel, C.; Boujtita, M.; Odobel, F. First Application of the HETPHEN Concept to new Heteroleptic bis (diimine) copper (I) Complexes as Sensitizers in Dye Sensitized Solar Cells. *Dalton Trans.* **2013**, *42*, 10818–10827.

(12) Kohler, L.; Hayes, D.; Hong, J.; Carter, T. J.; Shelby, M. L.; Fransted, K. A.; Chen, L. X.; Mulfort, K. L. Synthesis, Structure, Ultrafast Kinetics, and Light-induced Dynamics of CuHETPHEN Chromophores. *Dalton Trans.* **2016**, *45*, 9871–9883.

(13) Hayes, D.; Kohler, L.; Chen, L. X.; Mulfort, K. L. Ligand Mediation of Vectorial Charge Transfer in Cu (I) diimine Chromophore–Acceptor Dyads. *J. Phys. Chem. Lett.* **2018**, *9*, 2070–2076.

(14) Mara, M. W.; Phelan, B. T.; Xie, Z.-L.; Kim, T. W.; Hsu, D. J.; Liu, X.; Valentine, A. J. S.; Kim, P.; Li, X.; Adachi, S.-i. et al. Unveiling Ultrafast Dynamics in Bridged Bimetallic Complexes using Optical and X-ray Transient Absorption Spectroscopies. *Chem. Sci.* **2022**, *13*, 1715–1724.

(15) Hayes, D.; Kohler, L.; Hadt, R. G.; Zhang, X.; Liu, C.; Mulfort, K. L.; Chen, L. X. Excited State Electron and Energy Relays in Supramolecular Dinuclear Complexes Revealed by Ultrafast Optical and X-ray Transient Absorption Spectroscopy. *Chem. Sci.* **2018**, *9*, 860–875.

(16) Wasielewski, M. R. Photoinduced Electron Transfer in Supramolecular Systems for Artificial Photosynthesis. *Chem. Rev.* **1992**, *92*, 435–461.

(17) Ponseca Jr, C. S.; Chábera, P.; Uhlig, J.; Persson, P.; Sundström, V. Ultrafast Electron Dynamics in Solar Energy Conversion. *Chem. Rev.* **2017**, *117*, 10940–11024.

(18) Cheng, Y.-C.; Fleming, G. R. Dynamics of Light Harvesting in Photosynthesis. *Annu. Rev. Phys. Chem.* **2009**, *60*, 241–262.

(19) Li, X.; Govind, N.; Isborn, C.; DePrince, A. E.; Lopata, K. Real-Time Time-Dependent Electronic Structure Theory. *Chem. Rev.* **2020**, *120*, 9951–9993.

(20) Goings, J. J.; Lestrange, P. J.; Li, X. Real-Time Time-Dependent Electronic Structure Theory. *WIREs Comput. Mol. Sci.* **2018**, *8*, e1341.

(21) Li, X.; Tully, J. C.; Schlegel, H. B.; Frisch, M. J. Ab Initio Ehrenfest Dynamics. *J. Chem. Phys.* **2005**, *123*, 084106.

(22) Li, X.; Smith, S. M.; Markevitch, A. N.; Romanov, D. A.; Levis, R. J.; Schlegel, H. B. A Time-Dependent Hartree-Fock Approach for Studying the Electronic Optical Response of Molecules in Intense Fields. *Phys. Chem. Chem. Phys.* **2005**, *7*, 233–239.

(23) Isborn, C. M.; Li, X.; Tully, J. C. TDDFT Ehrenfest Dynamics: Collisions between Atomic Oxygen and Graphite Clusters. *J. Chem. Phys.* **2007**, *126*, 134307.

(24) Petrone, A.; Lingerfelt, D. B.; Rega, N.; Li, X. From Charge-Transfer to a Charge-Separated State: A Perspective from the Real-Time TDDFT Excitonic Dynamics. *Phys. Chem. Chem. Phys.* **2014**, *16*, 24457–24465.

(25) Ding, F.; Goings, J. J.; Liu, H.; Lingerfelt, D. B.; Li, X. Ab Initio Two-Component Ehrenfest Dynamics. *J. Chem. Phys.* **2015**, *143*, 114105.

(26) Donati, G.; Lingerfelt, D. B.; Petrone, A.; Rega, N.; Li, X. "Watching" Polaron Pair Formation from First-Principles Electron-Nuclear Dynamics. *J. Phys. Chem. A* **2016**, *120*, 7255–7261.

(27) Martin, R. L. Natural Transition Orbitals. *J. Chem. Phys.* **2003**, *118*, 4775–4777.

(28) Kasper, J. M.; Li, X. Natural Transition Orbitals for Complex Two-Component Excited State Calculations. *J. Comput. Chem.* **2020**, *41*, 1557–1563.

(29) Frisch, M. J.; Trucks, G. W.; Schlegel, H. B.; Scuseria, G. E.; Robb, M. A.; Cheeseman, J. R.; Scalmani, G.; Barone, V.; Petersson, G. A.; Nakatsuji, H. et al. Gaussian Development Version, Revision J.14+. Gaussian Inc. Wallingford CT 2020.

(30) Zhao, Y.; Truhlar, D. G. The M06 Suite of Density Functionals for Main Group Thermochemistry, Thermochemical Kinetics, Noncovalent Interactions, Excited States, and Transition Elements: Two New Functionals and Systematic Testing of Four M06-class Functionals and 12 Other Functionals. *Theor. Chem. Acc.* **2008**, *120*, 215–241.

(31) Grimme, S.; Antony, J.; Ehrlich, S.; Krieg, H. A Consistent and Accurate ab initio Parametrization of Density Functional Dispersion Correction (DFT-D) for the 94 Elements H-Pu. *J. Chem. Phys.* **2010**, *132*, 154104.

(32) Hay, P. J.; Wadt, W. R. Ab Initio Effective Core Potentials for Molecular Calculations. Potentials for the Transition Metal Atoms Sc to Hg. *J. Chem. Phys.* **1985**, *82*, 270–283.

(33) Pritchard, B. P.; Altarawy, D.; Didier, B.; Gibson, T. D.; Windus, T. L. New Basis Set Exchange: An Open, Up-to-Date Resource for the Molecular Sciences Community. *J. Chem. Inf. Model.* **2019**, *59*, 4814–4820.

(34) Stevens, W. J.; Basch, H.; Krauss, M. Compact Effective Potentials and Efficient Shared-exponent Basis Sets for the First- and Second-row Atoms. *J. Chem. Phys.* **1984**, *81*, 6026–6033.

(35) Fraser, M. G.; van der Salm, H.; Cameron, S. A.; Blackman, A. G.; Gordon, K. C. Heteroleptic Cu(I) Bis-diimine Complexes of 6,6′-Dimesityl-2,2′-bipyridine: A Structural, Theoretical and Spectroscopic Study. *Inorg. Chem.* **2013**, *52*, 2980–2992.

(36) Xie, Z.-L.; Liu, X.; Valentine, A. J. S.; Lynch, V. M.; Tiede, D. M.; Li, X.; Mulfort, K. L. Bimetallic Copper/Ruthenium/Osmium Complexes: Observation of Conformational Differences Between the Solution Phase and Solid State by Atomic Pair Distribution Function Analysis. *Angew. Chem. Int. Ed.* **2022**, *61*, e202111764.

(37) Mewes, S. A.; Dreuw, A. Density-based Descriptors and Exciton Analyses for Visualizing and Understanding the Electronic Structure of Excited States. *Phys. Chem. Chem. Phys.* **2019**, *21*, 2843–2856.

(38) Drummer, M. C.; Weerasooriya, R. B.; Gupta, N.; Askins, E. J.; Liu, X.; Valentine, A. J. S.; Li, X.; Glusac, K. D. Proton-Coupled Electron Transfer in a Ruthenium(II) Bipyrimidine Complex in Its Ground and Excited Electronic States. *J. Phys. Chem. A* **2022**, *126*, 4349–4358.

TOC Graphic